OCEANOGRAPHY

Nutrient ratios in marine particulate organic matter are predicted by the population structure of well-adapted phytoplankton

Shlomit Sharoni* and Itay Halevy*

A common assumption of a constant nitrogen-to-phosphorus ratio (N:P) of 16:1 in marine particulate organic matter (POM) appears to be invalidated by observations of major spatial variations in N:P. Two main explanations have been proposed. The first attributes the N:P variability to changes in the community composition of well-adapted phytoplankton. The second proposes that variability arises from physiological acclimation involving intracellular adjustments of nutrient allocation under nutrient deficiency. Using a model of phytoplankton physiology, observational datasets, and a review of laboratory culture results, we assess the mechanistic basis of N:P variability. We find that the taxonomic composition of well-adapted phytoplankton best explains observed variations in POM N:P. Furthermore, we show that acclimation to nutrient deficiency may be safely neglected when considering the effects of ecology on POM N:P. These findings provide insight into the controls on global variability in POM composition and average phytoplankton physiological performance in the oceans.

INTRODUCTION

The elemental composition of particulate organic matter (POM) dictates the flow of matter via the microbial food web and plays a key role in the biogeochemical cycles of carbon, oxygen, phosphorus, and nitrogen (*1*, *2*). Of particular interest are nitrogen (N) and phosphorus (P), which are essential macronutrients considered to limit marine primary production (*3*, *4*). In a seminal paper in 1934, Redfield proposed that the global spatial and temporal average C:N:P of POM (defined as the organic matter retained on 0.7-μm filters and composed mostly of phytoplankton cells) is constant and remarkably similar to the ratio of dissolved inorganic nutrients in the deep ocean, most likely as a result of the decomposition of POM into its constituents (*5*, *6*). A C:N:P of 106:16:1 in POM, the so-called Redfield ratio, has been fundamental in marine biogeochemistry for nearly a century (*7*, *8*). However, over the past decades, high-resolution measurements have revealed notable deviations of the N:P of POM in the oceans from the Redfield ratio, and a clear meridional N:P pattern is observed (*9*). For instance, the N:P of POM in the cold, nutrient-rich, high-latitude oceans is ~13:1, whereas in the warm, nutrient-depleted (oligotrophic), mid-latitude oceans, it is ~28:1, values that are respectively lower and higher than the Redfield ratio (*9*). Similar patterns have also been observed across seasons. N:P is higher in the summer (warm and nutrient-depleted) and lower in the winter (colder and nutrient-replete) at many sites (*10*–*12*). Identifying the mechanisms that underpin N:P variability is essential to understanding the factors that limit primary productivity, the effect of resource competition on community structure, and long-term regulation of ocean biogeochemistry (*3*, *13*).

Existing empirical research recognizes the critical role played by nutrients, namely, phosphate and nitrate, in controlling the meridional trend in POM stoichiometry (*1*). For instance, nutrient concentrations may affect the elemental composition of POM by controlling phytoplankton population structure (*9*). Diatoms require relatively nutrient-rich conditions and typically display lower-than-Redfield N:P. In contrast, cyanobacteria, which do well in nutrient-poor regions, display higher ratios under laboratory conditions (*14*–*16*). Thus, a diatom-dominated biomass, as generally observed at high latitudes, may explain low N:P in these locations, while cyanobacteria-dominated biomass may explain high N:P in oligotrophic systems. In addition, phenotypic plasticity due to acclimation of the phytoplankton to nitrate or phosphate limitation may lead to deviations in cellular stoichiometry (*17*). In this case, meridional variability may be related to the delivery of nitrate and phosphate to the photic zone, driven by ocean circulation patterns (*18*). Although changes in population structure and acclimation may lead to similar shifts in POM stoichiometry, they have different implications for the physiological state of the phytoplankton. Population structure shifts, involving spatiotemporal variations in the relative proportions of different groups, imply that the selected dominant phytoplankton are better adapted to the local nutrient availability and should thus display relatively high physiological fitness (i.e., high relative growth rate). On the other hand, acclimation involves a modification of cellular stoichiometry at the expense of fitness in response to environmental (nutrient) stress (*19*). Ecosystem health, as affected by the fitness of the primary producers, may have implications for the sensitivity of the biological pump to future changes in climate and nutrient delivery to the oceans (*20*).

The link between phytoplankton elemental composition, nutrient availability, and relative growth rate [i.e., the fraction of the maximum growth rate, which is an indication of physiological state (*21*)] is predicted by the "Droop" model, which describes the growth of phytoplankton in a chemostat (*22*–*24*). The solution of the Droop model shows that elemental composition of well-adapted cultures, growing rapidly under nutrient-replete conditions, converges on their optimal, species-specific ratio (Fig. 1, red points) (*14*–*17*, *25*, *26*). In this case, phytoplankton "eat what they need," retaining a homeostatic stoichiometry. On the other hand, the cellular composition of phytoplankton experiencing nutrient limitation may diverge from their optimal ratio during acclimation and their relative growth rate

Department of Earth and Planetary Sciences, Weizmann Institute of Science, Rehovot 76100, Israel.
*Corresponding author. Email: shlomit.sharoni@weizmann.ac.il (S.S.); itay.halevy@weizmann.ac.il (I.H.)

declines (*17*, *25*). In this case, phytoplankton "eat what they can," and their cellular N:P matches the N:P in the inorganic input medium over most of the input N:P range, and at low dilution (mortality) rates (Fig. 1, blue points). The modulation to nonoptimal cellular N:P occurs because of surplus accumulation of macromolecules enriched in nonlimiting nutrients, such as proteins under N surplus or polyphosphates under P surplus (*17*, *21*, *22*).

To test whether the meridional trend results from variations in the population structure of well-adapted phytoplankton or from the population structure of acclimated (nutrient-limited) cells, we integrated data on phytoplankton stoichiometry, growth, and nutrient uptake and developed a model to calculate the expected POM stoichiometry under nutrient-replete versus nitrate- or phosphate-limited growth (Materials and Methods). We then compared our calculated values to observations across all major oceanic basins. Our results strongly indicate that, on average, the taxonomic composition of well-adapted phytoplankton best explains observed variations in POM composition. Consequently, the N:P of POM can be predicted with good accuracy solely as a function of phytoplankton population structure.

RESULTS AND DISCUSSION

Deriving POM N:P from a model of nutrient uptake

The Droop model provides a mathematical framework that relates phytoplankton elemental composition, nutrient availability, and relative growth rate (*22*–*24*). The model follows the evolution of external nitrate and phosphate concentrations (N and P, respectively; μM), cellular N and P quotas (Q_N and Q_P, respectively; μmol cell^{-1}), and total cell biomass (X; cell liter^{-1}). Nutrients are supplied at the concentrations P_{in} and N_{in} (μM) and are taken up by the phytoplankton. Uptake of the nutrients follows a Michaelis-Menten saturating function form. Unused nutrients are washed out at a concentration identical to their concentration in the chemostat (or in the environment) and at the same rate of dilution (d; day^{-1}). Internal nutrient quotas increase by uptake and decrease by growth, which is limited by the nutrient in the shortest supply (*27*). The Droop equations are

$$\frac{dN}{dt} = d(N_{in} - N) - V_{max,N}\frac{N}{N + k_N}X \quad (1)$$

$$\frac{dP}{dt} = d(P_{in} - P) - V_{max,P}\frac{P}{P + k_P}X \quad (2)$$

$$\frac{dQ_N}{dt} = V_{max,N}\frac{N}{N + k_N} - \mu_\infty \min\left\{1 - \frac{Q_{min,N}}{Q_N}, 1 - \frac{Q_{min,P}}{Q_P}\right\}Q_N \quad (3)$$

$$\frac{dQ_P}{dt} = V_{max,P}\frac{P}{P + k_P} - \mu_\infty \min\left\{1 - \frac{Q_{min,N}}{Q_N}, 1 - \frac{Q_{min,P}}{Q_P}\right\}Q_P \quad (4)$$

$$\frac{dX}{dt} = \mu_\infty \min\left\{1 - \frac{Q_{min,N}}{Q_N}, 1 - \frac{Q_{min,P}}{Q_P}\right\}X - mX \quad (5)$$

where $V_{max,P}$ and $V_{max,N}$ are the maximum uptake rates (μmol cell^{-1} day^{-1}), k_N and k_P are the half-saturation constants (μM), μ_∞ is the growth rate at infinite quota (day^{-1}), m is the mortality rate (day^{-1}), and $Q_{min,N}$ and $Q_{min,P}$ are the minimum cellular quotas when growth is zero (μmol cell^{-1}). The Droop model can be simplified by assuming that, at any point in time, the ratio of nutrient uptake to carbon-based growth is in balance with the cellular quotas. In practice, this "balanced growth" assumption is achieved by assuming that the quotas adjust instantly to the environmental conditions and are in a quasi-steady state. It has been shown that this assumption is an accurate approximation of the full Droop model under a wide range of dynamic conditions (*28*). Therefore, the ratio of cellular N:P is obtained by equating the right-hand side of Eqs. 3 and 4 to zero, rearranging to solve for Q_N and Q_P, respectively, and dividing the resulting expressions to yield

$$(Q_N/Q_P) = (V_{max,N}/V_{max,P})\left(\frac{N}{N + k_N}\Big/\frac{P}{P + k_P}\right) \quad (6)$$

The cellular N:P ratio can then be calculated under three different scenarios to be tested, with the following three sets of assumptions:

(i) Phytoplankton in the field grow relatively rapidly, as they are adapted to the local nutrient supply. In this case, growth is unlimited by nutrient availability, i.e., the phytoplankton's half-saturation constants are significantly lower than in situ nutrient concentrations ($k_N << N$, $k_P << P$). Thus, the second term on the right-hand side of Eq. 6 is approximately unity. Furthermore, making the so-called optimal uptake assumption (*22*, *29*) that phytoplankton take up nutrients at an optimal ratio equal to the ratio of minimal cell quotas: $V_{max,N}/V_{max,P} = Q_{min,N}/Q_{min,P}$. Under these assumptions, Eq. 6 simplifies to

$$(\widetilde{Q}_N/\widetilde{Q}_P) = (Q_{min,N}/Q_{min,P}) \quad (7)$$

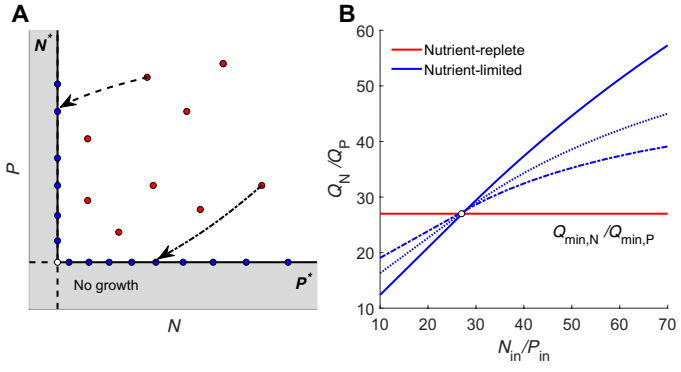

Fig. 1. Relation between phytoplankton elemental composition, nutrient availability, and relative growth rate according to the Droop model. (**A**) Schematic representation of the nutrient phase space. In the white area, phytoplankton are growing rapidly under nutrient-replete conditions (red dots). On the horizontal and vertical black lines, nutrient concentrations have been drawn down to low levels with final concentration P^* and N^* for a range of nutrient supply ratios. At these steady-state points (blue dots), phytoplankton are limited by phosphate and nitrate (*22*). The dashed and dashed-dotted trajectories represent a cell that becomes nitrate-limited ($N_{in} : P_{in} = 4 : 1$) and phosphate-limited ($N_{in} : P_{in} = 60 : 1$), respectively. In the gray zone, nutrients are below the minimal requirements for phytoplankton growth. (**B**) Cellular N:P stoichiometry as a function of nutrient input ratio and growth phase, calculated according to the Droop model, with parameters defined in table 2 in (*22*). Cellular N:P of nutrient-replete, exponentially growing phytoplankton converges on their optimum quotas independently of the nutrient input ratio (red line). Cellular N:P of phytoplankton growing under nutrient limitation is linearly correlated to the ratio of nutrient inputs at low dilution (mortality) rates ($d = 0.59$ day^{-1}; solid blue line) over most of the range shown. For higher dilution rates ($d = 0.9$, 1.0 day^{-1}; dotted and dashed blue lines, respectively), the curves become sigmoidal, revealing a limit to the flexibility of phytoplankton stoichiometry at high nutrient input ratio. The white dot represents the unique case in which the nutrient input ratio exactly matches the phytoplankton's optimal ratio.

where the tildes denote nutrient-unlimited (rapid) relative growth. This solution indicates that when nutrients are abundant, cellular N:P converges on the phytoplankton optimal group-specific ratio, which is equal to the ratio of the minimum nutrient quotas and independent of external nutrient concentrations. We label this strategy as the "optimal allocation" model (*14*–*16*, *22*). The expected cellular N:P under these conditions was calculated by substituting into the right-hand side of Eq. 7 the group-specific optimal N:P ($Q_{min,N}/Q_{min,P}$) extracted from the literature review (Fig. 2A and Table 1; Supplementary Materials).

(ii) Phytoplankton in the field acclimate to nutrient shortage (i.e., the second term on the right-hand side of Eq. 6 cannot be assumed to be unity) but take up nutrients at a ratio equal to the ratio of their minimum quotas (i.e., making the optimal uptake assumption). This is plausible for species that typically bloom in response to episodic nutrient inputs and that may partially acclimate to declining nutrient concentrations over the course of a bloom, without changing their uptake strategy (i.e., without adapting). In addition, this scenario is perhaps reasonable also for species that are pre-adapted to consume nutrients at the optimal ratio at low nutrient levels (*22*). By making this assumption, Eq. 6 becomes

$$(Q_N^*/Q_P^*) = (Q_{min,N}/Q_{min,P})\left(\frac{N}{N+k_N}\Big/\frac{P}{P+k_P}\right) \quad (8)$$

where the asterisks denote nutrient-limited growth. Equation 8 implies that under nitrate/phosphate limitation, the cellular N:P is lower/higher than the optimal ratio, respectively. It was shown that Eq. 8 predicts well the cellular N:P of phytoplankton cultures acclimated to nutrient-limited conditions (fig. S1) (*22*, *29*). We therefore labeled this strategy as the "cellular acclimation I" model. To calculate the expected cellular N:P under this assumption, we substitute into the right-hand side of Eq. 8 the group-specific optimal N:P ($Q_{min,N}/Q_{min,P}$) and half-saturation constants (k_N and k_P) from a literature review (Table 1 and table S2) and in situ N and P concentrations retrieved from the World Ocean Database (WOD) (*30*).

(iii) Phytoplankton in the field express maximum uptake rates and half-saturation constants similar to those measured in laboratory cultures acclimated to nutrient-limited conditions. We label this strategy the "cellular acclimation II" model. To calculate the expected cellular N:P under this assumption, we substitute into the right-hand side of Eq. 6 the group-specific kinetic parameters ($V_{max,N}$, $V_{max,P}$, k_N, and k_P) obtained from a literature review (table S2) and in situ N and P nutrient concentration retrieved from WOD.

The expected cellular N:P ratios were calculated according to scenarios (i) to (iii) and weighted by phytoplankton-group relative abundance retrieved from the NASA Ocean Biogeochemical Model (NOBM) (*31*, *32*) in every oceanographic domain (Eq. 9, Materials and Methods). To account for errors associated with the literature data, the nutrient concentration from WOD, and the phytoplankton relative-group abundance retrieved from NOBM, all of these parameters were repeatedly drawn (10,000 times) from distributions that represent uncertainties in their values. This results in a distribution of POM N:P predicted for every oceanographic region under each of the models, which was compared to observations.

To test cellular acclimation in isolation from phytoplankton population structure, we conducted two additional tests termed "cellular acclimation I only" and "cellular acclimation II only." For these tests, we use Eqs. 8 and 6, respectively, as described for scenarios (ii) and (iii), but we assume that one generic phytoplankton species dominates the ocean, with kinetic parameters and optimal stoichiometry that are a mean of the different phytoplankton groups. The results are presented in fig. S2.

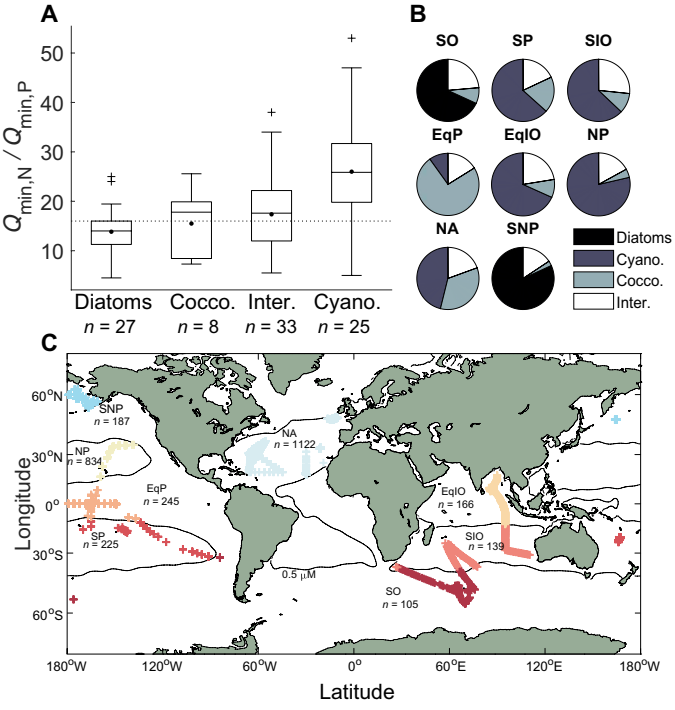

Fig. 2. N:P variations among phytoplankton phyla, phytoplankton group distributions, and geographic locations of sampling stations. (**A**) Cellular range of N:P (molar ratio) of the different phytoplankton groups. The dotted line is the Redfield ratio of 16:1. Phytoplankton groups are as in Table 1, and *n* is the number of observations. The box plots show the 25th, 50th, and 75th percentiles; the whiskers cover 99.3% of the data; the black dots are the mean; and the remaining outliers are shown as black crosses. Data are compiled from the literature on elemental stoichiometry of the different marine phytoplankton phyla under nutrient-sufficient growth conditions (table S1). (**B**) Pie charts represent the mean normalized relative phytoplankton group distribution data extracted from NOBM for the specific time and location of the N:P measurements. (**C**) Geographic locations of sampling stations, represented by the different colors, were clustered into oceanographic domains bounded by contours of 0.5 μM annual average phosphate concentration: the Southern Ocean (SO), South Pacific (SP), South Indian Ocean (SIO), Equatorial Pacific (EqP), Equatorial Indian Ocean (EqIO), North Pacific (NP), North Atlantic (NA), and Subarctic North Pacific (SNP). The analysis included only measurements from the upper 100 m of the water column, an approximation of the photic zone (*55*).

Group-specific N:P and phytoplankton biogeography

We used the framework described above to test whether the source of global variability in the N:P of POM across the major oceanic basins is driven primarily by phytoplankton population structure of well-adapted phytoplankton or from the population structure of nitrate/phosphate-limited cells. To achieve this, we compared the expected cellular N:P calculated according to scenarios (i) to (iii) (i.e., the optimal allocation and the cellular acclimation I and II models) to global observations of POM elemental composition (*33*, *34*).

The optimal allocation hypothesis implicitly assumes that phytoplankton in the field express their optimal group-specific N:P (Eq. 7), which is often measured in cultures growing under nutrient-replete conditions (*14*–*16*). Therefore, to calculate the expected N:P of bulk POM under the optimal allocation assumption, we convolved

Table 1. Elemental stoichiometry of the phytoplankton groups. N:P for diatoms (Bacillariophyceae, "Diatom"), coccolithophores ("Cocco."), intermediate group ("Inter."), which includes dinoflagellates and green algae, and cyanobacteria ("Cyano."). The complete dataset is available in table S1. Means (bold) and medians are in the top row. The 25th and 75th percentiles are in parentheses in the middle row. The number of observations (*n*) is in the bottom row.

	Diatom	Cocco.	Inter.	Cyano.
N:P	**14**, 14	**15**, 18	**17**, 18	**26**, 26
	(11, 16)	(8, 20)	(12, 22)	(20, 32)
n	27	5	33	25

taxon-specific elemental compositions from a new compilation of experimental data obtained by reviewing the existing literature, with global phytoplankton group distributions from the NOBM. On the basis of the literature review (table S1), we found that the elemental N:P of the different phytoplankton groups [diatoms, coccolithophores, cyanobacteria, and intermediates, which include dinoflagellates and green algae (*31*)] cultured under nutrient-replete, rapid-growth conditions significantly differ from each other [one-way analysis of variance (ANOVA), $P < 1.2 \times 10^{-5}$; Fig. 2A and Table 1]. These results highlight previously described intrinsic differences between the nutrient requirements of phytoplankton groups (*14*–*16*). For example, diatoms that require a high density of P-rich ribosomes for fast growth display low N:P, and coccolithophores and cyanobacteria that allocate large resources to nutrient uptake machinery such as enzymes and chloroplasts are N-rich but P-poor (*21*, *26*, *35*).

To predict the N:P of marine POM in scenarios (i) to (iii), the expected cellular N:P calculated under the three different scenarios must be weighted by the relative abundances of the various phytoplankton groups. We retrieved the relative abundances of the phytoplankton groups from NOBM in major oceanographic regions defined by 0.5 μM annual mean phosphate concentration contours (Fig. 2, B and C; Materials and Methods). We found that, during the measurement periods, diatoms dominate the biomass in the Subarctic North Pacific (SNP) and in the Southern Ocean (SO). Cyanobacteria exhibit the opposite behavior, dominating the biomass in the mid-latitude and the Southern Indian Ocean (SIO), and Equatorial Indian Ocean (EqIO). Coccolithophore relative abundance is high in the Equatorial Pacific (EqP) and in the North Atlantic (NA). Last, the intermediate group is the second most dominant group in the SIO and SO (Fig. 2B). Using the compiled N:P of phytoplankton groups and their relative abundances in the oceans, we determine the bulk elemental composition of POM under the optimal allocation model (an abundance-weighted average of the group-specific N:P; Materials and Methods).

To calculate the N:P expected under the alternative scenario, i.e., under the cellular acclimation models (I and II), we obtained the nitrate and phosphate concentrations from the WOD for every time and location in which an N:P measurement exists (fig. S3). We then used these nutrient concentrations with literature estimates of group-specific maximum uptake rates and half-saturation constants (table S2) to calculate cellular N:P under nutrient-limited conditions [scenarios (ii) and (iii); Eqs. 8 and 6, respectively]. Last, we also calculated the cellular N:P predicted by an empirical relationship between POM stoichiometry and nutrient concentrations in the oceans (*1*), using the nitrate and phosphate concentrations from the WOD (Supplementary Materials). We note that the mechanisms underlying this relationship are uncertain, but included it in the comparison in the hopes of shedding light on those mechanisms.

Expected N:P under the optimal allocation and the cellular acclimation models

In all models, the expected N:P values in each oceanographic region were calculated 10,000 times, repeatedly sampling from distributions representing the uncertainties associated with the group-specific N:P ratios, the kinetic constants, the oceanic nutrient concentrations from WOD, and the phytoplankton relative abundances from NOBM (table S2 and figs. S3 and S5). The expected POM N:P distributions calculated using the optimal allocation model (red bars in Fig. 3) show that in the SO and the SNP, which are mostly dominated by diatoms (Fig. 2B), the N:P means are lower than the Redfield ratio. On the other hand, in the SP (South Pacific), SIO, EqIO, NP (North Pacific), and NA, where cyanobacteria are the most dominant primary producers, N:P means are higher than the Redfield ratio.

The cellular acclimation I model (light blue bars in Fig. 3) predicts N:P in the SP, SIO, and NP that is lower than that predicted using the optimal allocation model (see Fig. 3 in the referred regions). If the parametrization of cellular acclimation I model (Eq. 8) is correct, this suggests that a significant fraction of the phytoplankton population in these regions experiences nitrate limitation. In contrast, in the SO, EqP, EqIO, NA, and SNP, the N:P in the nutrient-limited model is higher than the expected N:P in the optimal allocation model (see Fig. 3 in the referred regions). This suggests that a significant part of the population in these regions may be phosphate-limited. The cellular acclimation I only model (lighter blue bars, fig. S2) predicts N:P ratios that are close to the cellular acclimation I model but with lesser agreement with the observations ($r = -0.05$ and -0.28, respectively). The cellular acclimation II model and the cellular acclimation II only model predict POM N:P values of 1 to 10 (molar ratio), which are significantly lower than observations (dark blue bars in Fig. 3 and blue bars in fig. S2).

Comparison between model results and observations

We compared the optimal allocation and the cellular acclimation model predictions to the global observations (orange bars, Fig. 3) (*33*, *34*) and to the empirical relationship between aqueous nutrient concentrations and cellular N:P (white bars, Fig. 3) (*1*). We found that the expected N:P distributions calculated assuming the optimal allocation model are most similar to the observations in all the oceanographic regions (Pearson's correlation coefficient, $r = 0.80$; Fig. 3 and fig. S4). This similarity is highlighted by the small distances between the cumulative distribution functions calculated assuming the optimal allocation model and observations and the low relative variance (mean $\Delta = 0.26$, mean $\sigma = 0.14$; Table 2 and fig. S4). These values provide a slightly better fit to the observations than the distances between the cumulative distribution functions of the empirical relationship and the observations (mean $\Delta = 0.35$, mean $\sigma = 0.20$; Table 2 and fig. S4). We find that the expected N:P distributions calculated assuming the cellular acclimation I and II models agree least well with observations, displaying higher variances and higher distances between their cumulative distribution functions and those of the observations (mean $\Delta = 0.56$ and 0.86, mean $\sigma = 0.68$ and 0.70, respectively; Table 2 and fig. S4). Comparisons with a different regional clustering (0.4 and 0.6 μM phosphate

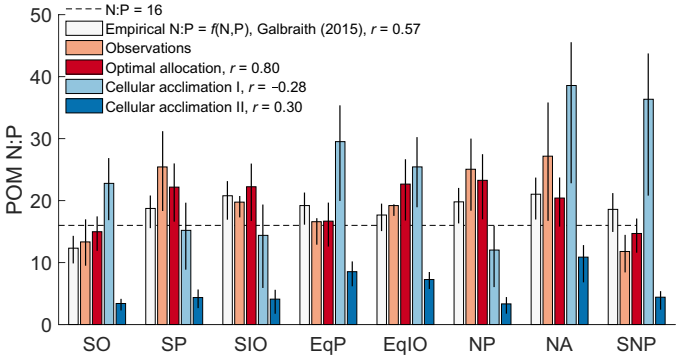

Fig. 3. Comparison between expected and observed POM N:P. The white bars represent the expected N:P calculated according to the empirical relationship of POM N:P and nutrient concentration described in (*1*). The orange bars represent the observed N:P across the different oceanographic basins (*33*, *34*). The red, light blue, and dark blue bars represent the expected N:P calculated according to the optimal allocation, cellular acclimation I, and cellular acclimation II models, respectively. The dashed black line represents the Redfield ratio. All data were clustered according to oceanographic regions defined in Fig. 2. The height of the bars represents the mean of the N:P distributions. The lower and upper black thick vertical lines are the 25th and 75th percentiles of the N:P distributions. *r* is the Pearson's correlation coefficient.

concentration contours) show that the results are robust to the exact choice of phosphate concentration as the cutoff among the different oceanographic domains (table S5).

The predictions of the cellular acclimation II model are strongly at odds with the observations. Similar differences between observed POM N:P and values calculated according to the cellular acclimation II model were also reported at the ALOHA (Pacific) and BATS (Atlantic) oceanographic stations (*36*). There are three possible reasons for this discrepancy: (i) the balanced growth approximation is not valid in the field, i.e., the cellular quotas are not in a quasi-steady state, (ii) the functional form of the model does not capture the growth of phytoplankton in the field, and/or (iii) the kinetic constants measured in the laboratory under nutrient-limited conditions do not apply to the real ocean. Option (i) is unlikely because phytoplankton populations typically equilibrate rapidly (*21*), although it is possible that further model analysis could reveal a long-term transient in cellular quotas. We find option (ii) unlikely, as myriad laboratory experiments have shown saturating nutrient uptake for a limiting nutrient and other functional forms have been found to yield similarly diverging calculations and observations (*36*). Option (iii), on the other hand, is supported by the observation that the half-saturation constant of *Prochlorococcus* cultures is 50 to 100 times higher than that of natural *Prochlorococcus* populations in the NP subtropical gyre (*37*, *38*). We refer the readers to (*36*) for further discussion regarding this discrepancy.

The good agreement between the POM N:P variability observed in the oceans and that predicted under the optimal allocation model suggests that this model, by itself, provides an adequate explanation of POM N:P variability across the different oceanographic regions and that adding the cellular acclimation does not improve the N:P predictions. Furthermore, the good agreement between the N:P distributions predicted by the empirical relationship, the observed distributions, and those predicted under the optimal allocation model suggests that the empirical relationship is similarly driven by the phytoplankton community structure. These findings suggest that phenotypic plasticity under nutrient limitation can be ignored when considering the controls on POM stoichiometry in most of the oceanographic regions, including the oligotrophic systems (Fig. 3). The only exception is in the NA, where the role of cellular plasticity in response to phosphate limitation is more readily observable. This is shown by the right tail of the N:P distribution (fig. S4), which indicates a degree of phenotypic N:P plasticity in response to P limitations. The detection of alkaline phosphatase activity in the NA provides evidence in support of the possibility that a fraction of the phytoplankton population experiences phosphate limitation (*39*).

Our results provide insights into the community dynamics in response to spatial and temporal variations in environmental conditions. Specifically, community dynamics is mainly dominated by variation in the relative proportions of different phytoplankton groups rather than by acclimation of any single group to the varying conditions. The suggested change in the phytoplankton assemblage in response to changes in environmental conditions is consistent with observations of algal bloom successions, in which specific taxa dominate over specific time intervals characterized by varying nutrient availability rather than acclimation of the phytoplankton standing stock to the varying conditions (*40*). Changes in community structure have also been shown to cause N:P variability in freshwater systems in response to temperature variations (*41*). Community structure, rather than cellular response to environmental stresses, was similarly shown to be a good predictor of spatial and temporal variations in the surface-ocean concentrations of dimethylsulfoniopropionate (DMSP), a bioactive organosulfur compound with several physiological roles, which is produced by phytoplankton (*42*).

A possible implication of our findings is that most of the phytoplankton population is not severely nutrient-limited, including in oligotrophic systems. We distinguish between two types of limitations: (i) "Blackman" limitation, which refers to a reduction in the growth rate of individual cells, and (ii) "Liebig" limitation, which refers to a reduction in the final yield of a population of cells (*3*, *43*). These two types of limitation are conceptually distinct, but their use is often vague in ecological studies (*43*). Our results indicate that phytoplankton in the oligotrophic systems, where phosphate and nitrate are often limiting (*3*), are not Blackman-limited, as indicated by the retention of average optimal group-specific elemental ratios. If this was not the case, under phosphate limitation, cellular N:P would be substantially higher than the groups' elemental ratios in nutrient-sufficient cultures, whereas under nitrate limitation cellular N:P would be lower than in cultures (fig. S1). Consequently, the calculated regional N:P based on the culture elemental ratios would not agree so well with the observed N:P. This said, the total yield in some cases can be low (i.e., Liebig limitation), as often shown by nutrient enrichment experiments (*3*), specifically in nutrient-poor settings in which the activity of grazers and viruses depresses phytoplankton biomass (*44*–*46*).

The suggestion that most phytoplankton are not stressed for nutrients in their natural environment agrees with classical views based on the results of rapid (relative) growth experiments and early POM measurements in the ocean (*25*). The apparent convergence of phytoplankton stoichiometry in rapid-growth experiments to the Redfield ratio, and the fact that this ratio was observed in marine measurements available at the time, led to the conclusion that the phytoplankton in the ocean grow relatively rapidly and are

Table 2. Comparison between expected and observed elemental N:P distributions. Δ represents the maximum distance between the cumulative distribution functions of the observations and the expected N:P distributions (Kolmogorov-Smirnov test). σ is the relative variance between the expected and observed distribution means, calculated according to Eq. 10 (Materials and Methods). Samples are from the upper 100 m of the water column, calculated in oceanographic regions defined by 0.5 μM annual average phosphate concentration contours.

Location	SO	SP	SIO	EqP	EqIO	NP	NA	SNP	Mean
Optimal allocation model—observations									
Δ	0.23	0.19	0.32	0.17	0.47	0.11	0.31	0.32	0.26
σ	0.12	0.13	0.13	0.01	0.17	0.07	0.25	0.25	0.14
Cellular acclimation I model—observations									
Δ	0.53	0.49	0.63	0.64	0.62	0.65	0.21	0.72	0.56
σ	0.71	0.40	0.26	0.80	0.33	0.53	0.42	2.05	0.68
Cellular acclimation II model—observations									
Δ	0.90	0.98	0.99	0.73	1.00	0.98	0.62	0.70	0.86
σ	0.74	0.83	0.80	0.49	0.62	0.87	0.59	0.63	0.70
Empirical—observations									
Δ	0.25	0.41	0.21	0.44	0.37	0.33	0.32	0.56	0.35
σ	0.08	0.26	0.05	0.15	0.08	0.21	0.23	0.58	0.20

not severely nutrient stressed (*25*). Using much larger datasets with global coverage and higher spatial resolution, our work provides observational support for these ideas. However, a conclusion of our study is that the Redfield ratio should not be treated as a single stoichiometric attractor but rather as the abundance-weighted sum of group-specific stoichiometry under nutrient-replete conditions.

We note that our observations are consistent with rapid relative growth rate of phytoplankton in the oceans, but they do not rule out the possibility that in much of the ocean algal populations experience an inadequate but serendipitously balanced (close to their weighted average optimum) nutrient supply ratio (i.e., the white marker in Fig. 1B). However, this seems unlikely, as circulation and turbulence on multiple spatial scales maintain a relatively uniform inorganic N:P in the deep ocean (*18*). Delivery to the surface during mixing of nutrients at this uniform N:P contradicts supply at ratios that coincidentally match the regional phytoplankton assemblage.

A possible limitation of our work is that we did not account for the potential contribution of dead autotrophic biomass, as well as for heterotrophs and bacteria, which can influence the elemental stoichiometry of marine POM (*47*, *48*). Although it was suggested that POM in the surface oligotrophic ocean is composed mostly of living cells (*9*), little is still known about the influence of heterotrophs and bacteria on the bulk POM stoichiometry. Furthermore, we focus on nitrate and phosphate, providing support for the impact of these major nutrients in marine ecosystems. However, our work has limited utility for assessing the effects of other limitations, such as iron limitation, which is thought to be important in wide oceanic areas (*43*, *49*). This is because the effect of iron limitation on phytoplankton stoichiometry is unclear. Different studies show either an increase, decrease, or no change in N:P of phytoplankton under iron stress, depending on growth conditions, growth stage, or algal strain used (*50*–*52*). Thus, the absence of a clear pattern of iron limitation on N:P stoichiometry does not allow clear assessment of the physiological state of phytoplankton with respect to iron availability, based on N:P of POM in the marine environment alone.

CONCLUSIONS

Our analysis provides further understanding of the role of phytoplankton communities on regulation of marine POM stoichiometry. Specifically, we show how such regulation can be achieved through spatiotemporal variations in the relative abundance of different groups displaying near-optimal physiological performance and elemental composition. Such recurrent selection of the well-adapted cells out of a diverse pool of genotypes likely sustains an effective flow of matter and energy through biogeochemical pathways. If so, the existence of a diverse pool of genotypes provides ecosystem resilience and ensures the transformation of inorganic carbon and nutrients into organic constituents and the transfer of these compounds across the marine food web under varying conditions at sea (*53*).

MATERIALS AND METHODS

Literature review

Group-specific data on N:P of marine phytoplankton under nutrient-sufficient conditions were extracted from the text, tables, and figures of 34 publications (250 data points in all). The database contains molar N:P, along with taxonomic information (class, species, and strain), culture conditions (batch, semicontinuous, or chemostat), medium type, temperature, irradiation, day length, and the technical procedure for measuring particulate organic P and N (e.g., spectral, high precision inductively coupled plasma mass spectrometry (HP-ICPMS), x-ray microanalysis, and nuclear magnetic resonance). In the analysis, we focused on marine Bacillariophyceae (diatoms), Prymnesiophyceae (coccolithophores), Dinophyceae (dinoflagellates),

Chlorophyceae and Prasinophyceae (green algae), and Cyanophyceae (cyanobacteria), representing five major marine phytoplankton classes (*14*). AlgaeBase, an online database of terrestrial, marine, and freshwater algae, was used to identify synonyms, phyla, and general environment. The literature review is available as the Supplementary Materials: "database_species_specific_stoichiometry.xlsx." Further details are in the Supplementary Materials.

Phytoplankton biogeography

The average monthly spatial distribution of major phytoplankton groups was retrieved from NOBM. NOBM is a three-dimensional representation of coupled physical transport, biogeochemical and radiative processes, at a spatial resolution of 1.25° longitude and 0.66° latitude, spanning a range of latitudes between −84° and +72°, and including only open-ocean areas where seafloor depth is >200 m. The biogeochemical model contains four phytoplankton groups [diatoms, coccolithophores, intermediate (including chlorophytes and dinoflagellates), and cyanobacteria] and four nutrient groups (nitrate, ammonia, silica, and iron). Phytoplankton biomass in a certain location is determined by a balance between group-specific sinking rates and growth rates, the latter of which depend on group-specific nutrient and light requirements and the nutrient concentrations and optical properties of the photic zone. Growth and succession of the different phytoplankton groups is simulated in this model by trait-based differences of the phytoplankton groups: maximum growth rate, sinking rate, and half-saturation constants to nutrients and light. Phytoplankton stoichiometry is fixed at the Redfield ratio, with a light adaptation (variable C:Chl ratio) formulation. The model provides phytoplankton group biomass calculated for monthly average oceanographic conditions starting in 1998 (*31*).

Because our estimates of relative phytoplankton abundance are derived from NOBM, it is possible that our results are biased by NOBM underlying assumptions (for example, four functional groups and four limiting nutrients). However, to our knowledge, NOBM is the most established coupled ocean biogeochemical model simulating the distribution of the different phytoplankton groups, and its global and temporal extent enables us to couple predictions of phytoplankton group distribution with observations of POM N:P. The model was validated against 469 surface-layer observations of phytoplankton group abundance. With the exception of the intermediate group, the model reproduces well the distributions of coccolithophores, diatoms, and cyanobacteria (*32*). Furthermore, NOBM has been extensively validated by other parameters involving a comparison of 9 of the 14 model state variables against in situ and/or satellite datasets (only the abundance of herbivores, the three detrital components, and dissolved organic carbon have not been validated). Moreover, diatoms and cyanobacteria retrieved from NOBM show good agreement with PhytoDOAS, which is a remote-sensing method to derive the relative abundance and biomass of diatoms and cyanobacteria using spectral methods (*54*). Furthermore, phosphate availability, which is an important component regulating cellular N:P, does not influence the calculations in NOBM, yet the expected N:P calculated by convolving NOBM community composition and laboratory N:P nicely predicts the observed N:P in nearly all ocean regions (Fig. 3).

Calculation of POM N:P in the different oceanographic regions

All the expected Q_N/Q_P in scenarios (i) to (iii) (Eqs. 6 to 8) were calculated for each group according to the group-specific parameters and then weighted by their relative contribution to the total biomass in the different oceanographic domains by the following equation

$$(N/P)_j = \frac{\sum_{g=1}^{n} f_{j,g} \times (N/P)_{expected,g}}{\sum_{g=1}^{n} f_{j,g}} \quad (9)$$

where $f_{j,g}$ is the mean relative abundance of the phytoplankton g group (g = diatoms, coccolithophores, intermediates, and cyanobacteria) in region j (j = SO, SIO, EP, etc.) extracted from NOBM, n is the number of phytoplankton groups, and $(N/P)_{expected,\,g}$ was calculated according to the different models (Eqs. 6 to 8). There is an uncertainty in the values of $Q_{min,N}/Q_{min,P}$, k_N, k_P, $V_{max,N}$, and $V_{max,P}$ because these parameters represent an average over different strains and laboratory conditions. Furthermore, there is an uncertainty regarding the nitrate and phosphate concentration retrieved from WOD, especially in the oligotrophic regions. To account for all these uncertainties, we performed 10,000 calculations with these parameters drawn from distributions that represent the uncertainty in their values (fig. S3 and table S2). Furthermore, there is an uncertainty associated with the relative abundance of the phytoplankton groups retrieved from NOBM. Therefore, during the simulations, this error was also drawn from normal distributions (fig. S5), and $f_{j,g}$ was corrected: $f_{j,g} = f_{j,g}$ − error (Supplementary Materials). The normal distributions of the errors were constructed using the mean and SD of the global error [model − observation; figure 6 in (*32*); fig. S5]. This resulted in distributions of expected N:P values under the different scenarios: (i) optimal allocation, (ii) cellular acclimation I, and (iii) cellular acclimation II. We also calculated the expected POM N:P according to the empirical relationship between nutrient concentrations and POM stoichiometry (Supplementary Materials) (*1*).

Comparison between expected and observed N:P

To compare expected N:P from the NOBM phytoplankton group composition to in situ data from measurements over the years 1974–2016 (*33*, *34*), we retrieved the phytoplankton group distributions from NOBM for every time and location in which N:P measurements were made and calculated the expected N:P distributions. For samples taken before 1998, for which oceanographic data do not exist in NOBM, we used the monthly mean oceanographic data from 2004, which is the year with the minimal sum of deviations from the monthly mean (Supplementary Materials). The observational database contains a total of 49,292 samples from cruises and marine stations that are distributed globally. We only considered samples from the upper 100 m of the water column, representing the average mixed layer (*55*), for which N and P data were determined in the same measurements and excluded samples in which particulate organic P concentrations were less than 5 nM, as this was the reported practical detection limit (*9*). After this screening, we were left with 3490 observational data points. We calculated the observed bulk elemental N:P distributions of the POM in eight oceanographic regimes confined by contours of annual average phosphate concentrations of 0.5 μM and compared to the average bulk N:P calculated from the NOBM distributions (tables S3 to S5). We excluded (i) the South and Equatorial Atlantic where the number of measurements was small (n < 11), (ii) measurements

with proximity to continents, and (iii) measurements in the Mediterranean Sea ($n = 458$), which are heavily influenced by riverine inputs. The relative variance between the expected mean and the observation mean was calculated according to the following equation

$$S = \left| \frac{(Q_N/Q_P)_j - (Q_N/Q_P)_j'}{(Q_N/Q_P)_j'} \right| \quad (10)$$

where S (%) is the relative variance between the expected and observed value, $(Q_N/Q_P)_j$ is the mean expected N:P in a region j, and $(Q_N/Q_P)_j'$ is the mean observed N:P in a region j.

SUPPLEMENTARY MATERIALS

Supplementary material for this article is available at http://advances.sciencemag.org/cgi/content/full/6/29/eaaw9371/DC1

REFERENCES AND NOTES

1. E. D. Galbraith, A. C. Martiny, A simple nutrient-dependence mechanism for predicting the stoichiometry of marine ecosystems. *Proc. Nat. Acad. Sci. U.S.A.* **112**, 8199–8204 (2015).
2. T. Tanioka, K. Matsumoto, Buffering of ocean export production by flexible elemental stoichiometry of particulate organic matter. *Global Biogeochem. Cycles* **31**, 1528–1542 (2017).
3. C. M. Moore, M. M. Mills, K. R. Arrigo, I. Berman-Frank, L. Bopp, P. W. Boyd, E. D. Galbraith, R. J. Geider, C. Guieu, S. L. Jaccard, T. D. Jickells, J. La Roche, T. M. Lenton, N. M. Mahowald, E. Marañón, I. Marinov, J. K. Moore, T. Nakatsuka, A. Oschlies, M. A. Saito, T. F. Thingstad, A. Tsuda, O. Ulloa, Processes and patterns of oceanic nutrient limitation. *Nat. Geosci.* **6**, 701–710 (2013).
4. W.-L. Wang, J. K. Moore, A. C. Martiny, F. W. Primeau, Convergent estimates of marine nitrogen fixation. *Nature* **566**, 205–211 (2019).
5. A. C. Redfield, *On the Proportions of Organic Derivatives in Sea Water and Their Relation to the Composition of Plankton* (University Press of Liverpool, 1934).
6. A. C. Redfield, The biological control of chemical factors in the environment. *Am. Sci.* **46**, 205–221 (1958).
7. N. J. Antia, C. D. McAllister, T. R. Parsons, K. Stephens, J. D. H. Strickland, Further measurements of primary production using a large-volume plastic sphere. *Limnol. Oceanogr.* **8**, 166–183 (1963).
8. M. J. Perry, Phosphate utilization by an oceanic diatom in phosphorus-limited chemostat culture and in the oligotrophic waters of the central North Pacific. *Limnol. Oceanogr.* **21**, 88–107 (1976).
9. A. C. Martiny, C. T. Pham, F. W. Primeau, J. A. Vrugt, J. K. Moore, S. A. Levin, M. W. Lomas, Strong latitudinal patterns in the elemental ratios of marine plankton and organic matter. *Nat. Geosci.* **6**, 279–283 (2013).
10. A. C. Martiny, A. Talarmin, C. Mouginot, J. A. Lee, J. S. Huang, A. G. Gellene, D. A. Caron, Biogeochemical interactions control a temporal succession in the elemental composition of marine communities. *Limnol. Oceanogr.* **61**, 531–542 (2016).
11. A. Singh, S. E. Baer, U. Riebesell, A. C. Martiny, M. W. Lomas, C : N : P stoichiometry at the Bermuda Atlantic time-series study station in the North Atlantic ocean. *Biogeosciences* **12**, 6389–6403 (2015).
12. A. Talarmin, M. W. Lomas, Y. Bozec, N. Savoye, H. Frigstad, D. M. Karl, A. C. Martiny, Seasonal and long-term changes in elemental concentrations and ratios of marine particulate organic matter. *Global Biogeochem. Cycles* **30**, 1699–1711 (2016).
13. D. Tilman, *Resource Competition and Community Structure* (Princeton Univ. Press, 1982).
14. T.-Y. Ho, A. Quigg, Z. V. Finkel, A. J. Milligan, K. Wyman, P. G. Falkowski, F. M. Morel, The Elemental composition of some marine phytoplankton. *J. Phycol.* **39**, 1145–1159 (2003).
15. A. Quigg, Z. V. Finkel, A. J. Irwin, Y. Rosenthal, T.-Y. Ho, J. R. Reinfelder, O. Schofield, F. M. Morel, P. G. Falkowski, The evolutionary inheritance of elemental stoichiometry in marine phytoplankton. *Nature* **425**, 291–294 (2003).
16. S. Bertilsson, O. Berglund, D. M. Karl, S. W. Chisholm, Elemental composition of marine *Prochlorococcus* and *Synechococcus*: Implications for the ecological stoichiometry of the sea. *Limnol. Oceanogr.* **48**, 1721–1731 (2003).
17. G.-Y. Rhee, Effects of N:P atomic ratios and nitrate limitation on algal growth, cell composition, and nitrate uptake. *Limnol. Oceanogr.* **23**, 10–25 (1978).
18. T. S. Weber, C. Deutsch, Ocean nutrient ratios governed by plankton biogeography. *Nature* **467**, 550–554 (2010).
19. A. R. Moreno, A. C. Martiny, Ecological stoichiometry of ocean plankton. *Ann. Rev. Mar. Sci.* **10**, 43–69 (2018).
20. A. R. Moreno, G. I. Hagstrom, F. W. Primeau, S. A. Levin, A. C. Martiny, Marine phytoplankton stoichiometry mediates nonlinear interactions between nutrient supply, temperature, and atmospheric CO_2. *Biogeosciences* **15**, 2761–2779 (2018).
21. R. W. Sterner, J. J. Elser, *Ecological Stoichiometry: The Biology of Elements from Molecules to the Biosphere* (Princeton Univ. Press, 2002).
22. C. A. Klausmeier, E. Litchman, S. A. Levin, Phytoplankton growth and stoichiometry under multiple nutrient limitation. *Limnol. Oceanogr.* **49**, 1463–1470 (2004).
23. M. R. Droop, Vitamin B12 and marine ecology. IV. The kinetics of uptake, growth and inhibition in Monochrysis lutheri. *J. Mar. Biol. Assoc.* **48**, 689–733 (1968).
24. M. R. Droop, Some thoughts on nutrient limitation in algae. *J. Phycol.* **9**, 264–272 (1973).
25. J. C. Goldman, J. J. McCarthy, D. G. Peavey, Growth rate influence on the chemical composition of phytoplankton in oceanic waters. *Nature* **279**, 210–215 (1979).
26. C. A. Klausmeier, E. Litchman, T. Daufresne, S. A. Levin, Optimal nitrogen-to-phosphorus stoichiometry of phytoplankton. *Nature* **429**, 171–174 (2004).
27. H. de Baar, von Liebig's law of the minimum and plankton ecology (1899–1991). *Prog. Oceanogr.* **33**, 347–386 (1994).
28. B. A. Ward, Assessing an efficient "Instant Acclimation" approximation of dynamic phytoplankton stoichiometry. *J. Plankton Res.* **39**, 803–814 (2017).
29. C. A. Klausmeier, E. Litchman, S. A. Levin, A model of flexible uptake of two essential resources. *J. Theor. Biol.* **246**, 278–289 (2007).
30. T. P. Boyer, J. I. Antonov, O. K. Baranova, C. Coleman, H. E. Garcia, A. Grodsky, D. R. Johnson, R. A. Locarnini, A. V. Mishonov, T. D. O'Brien, C. R. Paver, J. R. Reagan, D. Seidov, I. V. Smolyar, M. M. Zweng, World Ocean Database 2013, *NOAA Atlas NESDIS 72*, S. Levitus, Ed; A. Mishonov, Technical Ed. (Silver Spring, MD, USA, 2013), 209 pp.
31. W. W. Gregg, P. Ginoux, P. S. Schopf, N. W. Casey, Phytoplankton and iron: Validation of a global three-dimensional ocean biogeochemical model. *Deep Sea Res. Part 2 Top. Stud. Oceanogr.* **50**, 3143–3169 (2003).
32. W. W. Gregg, N. W. Casey, Modeling coccolithophores in the global oceans. *Deep Sea Res. Part 2 Top. Stud. Oceanogr.* **54**, 447–477 (2007).
33. A. C. Martiny, J. A. Vrugt, M. W. Lomas, Concentrations and ratios of particulate organic carbon, nitrogen, and phosphorus in the global ocean. *Sci. Data* **1**, 140048 (2014).
34. C. A. Garcia, S. E. Baer, N. S. Garcia, S. Rauschenberg, B. S. Twining, M. W. Lomas, A. C. Martiny, Nutrient supply controls particulate elemental concentrations and ratios in the low latitude eastern Indian Ocean. *Nat. Commun.* **9**, 4868 (2018).
35. Z. V. Finkel, M. J. Follows, J. D. Liefer, C. M. Brown, I. Benner, A. J. Irwin, Phylogenetic diversity in the macromolecular composition of microalgae. *PLOS ONE* **11**, e0155977 (2016).
36. F. I. Ballantyne, D. N. Menge, J. S. Weitz, A discrepancy between predictions of saturating nutrient uptake models and nitrogen-to-phosphorus stoichiometry in the surface ocean. *Limnol. Oceanogr.* **55**, 997–1008 (2010).
37. K. M. Björkman, S. Duhamel, D. M. Karl, Microbial group specific uptake kinetics of inorganic phosphate and adenosine-5′-triphosphate (ATP) in the north pacific subtropical gyre. *Front. Microbiol.* **3**, 189 (2012).
38. K. M. Krumhardt, K. Callnan, K. Roache-Johnson, T. Swett, D. Robinson, E. N. Reistetter, J. K. Saunders, G. Rocap, L. R. Moore, Effects of phosphorus starvation versus limitation on the marine cyanobacterium *Prochlorococcus* MED4 I: Uptake physiology. *Environ. Microbiol.* **15**, 2114–2128 (2013).
39. M. Vidal, C. M. Duarte, S. Agustí, J. M. Gasol, D. Vaqué, Alkaline phosphatase activities in the central Atlantic Ocean indicate large areas with phosphorus deficiency. *Mar. Ecol. Prog. Ser.* **262**, 43–53 (2003).
40. S. Alvain, C. Moulin, Y. Dandonneau, H. Loisel, Seasonal distribution and succession of dominant phytoplankton groups in the global ocean: A satellite view. *Global Biogeochem. Cycles* **22**, GB3001 (2008).
41. C. S. Reynolds, *The Ecology of Phytoplankton* (Cambridge Univ. Press, 2006).
42. E. L. McParland, N. M. Levine, The role of differential DMSP production and community composition in predicting variability of global surface DMSP concentrations. *Limnol. Oceanogr.* **64**, 757–773 (2019).
43. J. J. Cullen, X. Yang, H. L. MacIntyre, in *Primary Productivity and Biogeochemical Cycles in the Sea* (Springer, 1992), pp. 69–88.
44. M. V. Zubkov, Faster growth of the major prokaryotic versus eukaryotic CO_2 fixers in the oligotrophic ocean. *Nat. Commun.* **5**, 3776 (2014).
45. M. Mühling, N. J. Fuller, A. Millard, P. J. Somerfield, D. Marie, W. H. Wilson, D. J. Scanlan, A. F. Post, I. Joint, N. H. Mann, Genetic diversity of marine *Synechococcus* and co-occurring cyanophage communities: Evidence for viral control of phytoplankton. *Environ. Microbiol.* **7**, 499–508 (2005).
46. K. D. Mojica, J. Huisman, S. W. Wilhelm, C. P. Brussaard, Latitudinal variation in virus-induced mortality of phytoplankton across the North Atlantic Ocean. *ISME J.* **10**, 500–513 (2016).
47. D. Talmy, A. Martiny, C. Hill, A. Hickman, M. Follows, Microzooplankton regulation of surface ocean POC:PON ratios. *Global Biogeochem. Cycles* **30**, 311–332 (2016).

48. H. Frigstad, T. Andersen, D. O. Hessen, L.-J. Naustvoll, T. M. Johnsen, R. Bellerby, Seasonal variation in marine C:N:P stoichiometry: Can the composition of seston explain stable Redfield ratios? *Biogeosciences* **8**, 2917–2933 (2011).
49. J. H. Martin, Glacial-interglacial CO_2 change: The iron hypothesis. *Paleoceanogr. Paleoclimatol.* **5**, 1–13 (1990).
50. R. M. Greene, R. J. Geider, P. G. Falkowski, Effect of iron limitation on photosynthesis in a marine diatom. *Limnol. Oceanogr.* **36**, 1772–1782 (1991).
51. J. G. Rueler, D. R. Ades, The role of iron nutrition in photosynthesis and nitrogen assimilation in *Scenedesmus Quadricauda* (Chlorophyceae). *J. Phycol.* **23**, 452–457 (1987).
52. S. Takeda, Influence of iron availability on nutrient consumption ratio of diatoms in oceanic waters. *Nature* **393**, 774–777 (1998).
53. D. U. Hooper, F. S. Chapin III, J. J. Ewel, A. Hector, P. Inchausti, S. Lavorel, J. H. Lawton, D. Lodge, M. Loreau, S. Naeem, B. Schmid, H. Setälä, A. J. Symstad, J. Vandermeer, D. A. Wardle, Effects of biodiversity on ecosystem functioning: A consensus of current knowledge. *Ecol. Monogr.* **75**, 3–35 (2005).
54. A. Bracher, M. Vountas, T. Dinter, J. Burrows, R. Röttgers, I. Peeken, Quantitative observation of cyanobacteria and diatoms from space using PhytoDOAS on SCIAMACHY data. *Biogeosciences* **6**, 751–764 (2009).
55. C. de Boyer Montégut, G. Madec, A. S. Fischer, A. Lazar, D. Iudicone, Mixed layer depth over the global ocean: An examination of profile data and a profile-based climatology. *J. Geophys. Res.* **109**, C12003 (2004).
56. E. Litchman, C. Klausmeier, J. Miller, O. Schofield, P. Falkowski, Multi-nutrient, multi-group model of present and future oceanic phytoplankton communities. *Biogeosciences* **3**, 585–606 (2006).
57. K. Timmermans, B. van der Wagt, M. Veldhuis, A. Maatman, H. de Baar, Physiological responses of three species of marine pico-phytoplankton to ammonium, phosphate, iron and light limitation. *J. Sea Res.* **53**, 109–120 (2005).
58. F.-X. Fu, Y. Zhang, Y. Feng, D. A. Hutchins, Phosphate and ATP uptake and growth kinetics in axenic cultures of the cyanobacterium *Synechococcus* CCMP 1334. *Eur. J. Phycol.* **41**, 15–28 (2006).
59. E. Marañón, P. Cermeño, D. C. López-Sandoval, T. Rodríguez-Ramos, C. Sobrino, M. Huete-Ortega, J. M. Blanco, J. Rodríguez, Unimodal size scaling of phytoplankton growth and the size dependence of nutrient uptake and use. *Ecol. Lett.* **16**, 371–379 (2013).
60. A. Brutemark, E. Lindehoff, E. Granéli, W. Granéli, Carbon isotope signature variability among cultured microalgae: Influence of species, nutrients and growth. *J. Exp. Mar. Biol. Ecol.* **372**, 98–105 (2009).
61. A. Corcoran, B. Richardson, L. J. Flewelling, Effects of nutrient-limiting supply ratios on toxin content of *Karenia brevis* grown in continuous culture. *Harmful Algae* **39**, 334–341 (2014).
62. G. O. Fistarol, C. Legrand, E. Granéli, Allelopathic effect on a nutrient-limited phytoplankton species. *Aquat. Microb. Ecol.* **41**, 153–161 (2005).
63. F.-X. Fu, Y. Zhang, K. Leblanc, S. A. Sañudo-Wilhelmy, D. A. Hutchins, The biological and biogeochemical consequences of phosphate scavenging onto phytoplankton cell surfaces. *Limnol. Oceanogr.* **50**, 1459–1472 (2005).
64. F. X. Fu, Y. Zhang, P. R. Bell, D. A. Hutchins, Phosphate uptake and growth kinetics of *Trichodesmium* (cyanobacteria) isolates from the North Atlantic Ocean and the great barrier REEF, Australia. *J. Phycol.* **41**, 62–73 (2005).
65. F.-X. Fu, Y. Zhang, M. E. Warner, Y. Feng, J. Sun, D. A. Hutchins, A comparison of future increased CO_2 and temperature effects on sympatric *Heterosigma akashiwo* and *Prorocentrum minimum*. *Harmful Algae* **7**, 76–90 (2008).
66. N. S. Garcia, J. A. Bonachela, A. C. Martiny, Interactions between growth-dependent changes in cell size, nutrient supply and cellular elemental stoichiometry of marine *Synechococcus*. *ISME J.* **11**, 2715–2724 (2016).
67. N. S. Garcia, J. Sexton, T. Riggins, J. Brown, M. W. Lomas, A. C. Martiny, High variability in cellular stoichiometry of carbon, nitrogen, and phosphorus within classes of marine eukaryotic phytoplankton under sufficient nutrient conditions. *Front. Microbiol.* **9**, 543 (2018).
68. J. C. Goldman, D. A. Caron, M. R. Dennett, Nutrient cycling in a microflagellate food chain: IV. Phytoplankton-microflagellate interactions. *Mar. Ecol. Prog. Ser.* **38**, 75–87 (1987).
69. J. C. Goldman, D. A. Hansell, M. Dennett, Chemical characterization of three large oceanic diatoms: Potential impact on water column chemistry. *Mar. Ecol. Prog. Ser.* **88**, 257–270 (1992).
70. C. M. Holl, J. P. Montoya, Diazotrophic growth of the marine cyanobacterium *Trichodesmium* IMS101 in continuous culture: Effects of growth rate on N_2-Fixation rate, biomass, and C:N:P stoichiometry. *J. Phycol.* **44**, 929–937 (2008).
71. N. Johansson, E. Granéli, Cell density, chemical composition and toxicity of *Chrysochromulina polylepis* (Haptophyta) in relation to different N:P supply ratios. *Mar. Biol.* **135**, 209–217 (1999).
72. A. Kremp, K. Rengefors, M. Montresorc, Species specific encystment patterns in three Baltic cold-water dinoflagellates: The role of multiple cues in resting cyst formation. *Limnol. Oceanogr.* **54**, 1125–1138 (2009).
73. C. B. Kretz, D. W. Bell, D. A. Lomas, M. W. Lomas, A. C. Martiny, Influence of growth rate on the physiological response of marine *Synechococcus* to phosphate limitation. *Front. Microbiol.* **6**, (2015).
74. C. Labry, E. Erard-LeDenn, A. Chapelle, J. Fauchot, A. Youenou, M. P. Crassous, J. Le Grant, B. Lorgeoux, Competition for phosphorus between two dinoflagellates: A toxic *Alexandrium minutum* and a non-toxic *Heterocapsa triquetra*. *J. Exp. Mar. Biol. Ecol.* **358**, 124–135 (2008).
75. S. Lehtinen, S. Sopanen, T. Tamminen, Community-level and species-specific responses of coastal phytoplankton to the presence of two mesozooplanktonic grazers. *Mar. Biol.* **157**, 1555–1565 (2010).
76. J. S. Lopez, N. S. Garcia, D. Talmy, A. C. Martiny, Diel variability in the elemental composition of the marine cyanobacterium *Synechococcus*. *J. Plankton Res.* **38**, 1052–1061 (2016).
77. B. A. McKew, G. Metodieva, C. A. Raines, M. V. Metodiev, R. J. Geider, Acclimation of *Emiliania huxleyi* (1516) to nutrient limitation involves precise modification of the proteome to scavenge alternative sources of N and P. *Environ. Microbiol.* **17**, 4050–4062 (2015).
78. C. Mouginot, A. E. Zimmerman, J. A. Bonachela, H. Fredricks, S. D. Allison, B. A. Van Mooy, A. C. Martiny, Resource allocation by the marine cyanobacterium *Synechococcus* WH 8102 in response to different nutrient supply ratios. *Limnol. Oceanogr.* **60**, 1634–1641 (2015).
79. T. R. Parsons, K. Stephens, J. D. H. Strickland, On the chemical composition of eleven species of marine phytoplankters. *J. Fish. Board Can.* **18**, 1001–1016 (1961).
80. A. Quigg, A. J. Irwin, A. Z. V. Finkel, Evolutionary inheritance of elemental stoichiometry in phytoplankton. *Proc. R. Soc. B* **278**, 526–534 (2010).
81. E. M. Saad, A. F. Longo, L. R. Chambers, R. Huang, C. Benitez-Nelson, S. T. Dyhrman, J. M. Diaz, Y. Tang, E. D. Ingall, Understanding marine dissolved organic matter production: Compositional insights from axenic cultures of *Thalassiosira pseudonana*. *Limnol. Oceanogr.* **61**, 2222–2233 (2016).
82. E. Sakshaug, K. Andresen, S. Myklestad, Y. Olsen, Nutrient status of phytoplankton communities in Norwegian waters (marine, brackish, and fresh) as revealed by their chemical composition. *J. Plankton Res.* **5**, 175–196 (1983).
83. S. A. Sañudo-Wilhelmy, A. Tovar-Sanchez, F.-X. Fu, D. G. Capone, E. J. Carpenter, D. A. Hutchins, The impact of surface-adsorbed phosphorus on phytoplankton Redfield stoichiometry. *Nature* **432**, 897–901 (2004).
84. K. Spilling, P. Ylöstalo, S. Simis, J. Seppälä, Interaction effects of light, temperature and nutrient limitations (N, P and Si) on growth, stoichiometry and photosynthetic parameters of the cold-water diatom *Chaetoceros wighamii*. *PLOS ONE* **10**, e0126308 (2015).
85. N. K. Vidyarathna, E. Granéli, Physiological responses of *Ostreopsis ovata* to changes in N and P availability and temperature increase. *Harmful Algae* **21–22**, 54–63 (2013).
86. A. E. White, Y. H. Spitz, D. M. Karl, R. M. Letelier, Flexible elemental stoichiometry in *Trichodesmium* spp. and its ecological implications. *Limnol. Oceanogr.* **51**, 1777–1790 (2006).

Acknowledgments: We thank B. Ward and an anonymous reviewer for comments and criticisms, which improved the manuscript. We thank M. Frada, Y. Lehahn, and G. Watson for discussions and the Interuniversity Institute for Marine Sciences in Eilat for hosting us. **Funding:** S.S. acknowledges support from the Rieger Foundation of the Jewish National Fund. I.H. acknowledges European Research Council Starting Grant 337183. **Author contributions:** S.S. and I.H. conceived and designed the study. S.S. compiled the experimental and observational data and performed the analysis. I.H. oversaw the research. S.S. and I.H. wrote the paper. **Competing interests:** The authors declare that they have no competing interests. **Data and materials availability:** All data needed to evaluate the conclusions in the paper are present in the paper and/or the Supplementary Materials. Additional data related to this paper may be requested from the authors.

Submitted 9 September 2019
Accepted 2 June 2020
Published 15 July 2020
10.1126/sciadv.aaw9371

Citation: S. Sharoni, I. Halevy, Nutrient ratios in marine particulate organic matter are predicted by the population structure of well-adapted phytoplankton. *Sci. Adv.* **6**, eaaw9371 (2020).

Science Advances

Nutrient ratios in marine particulate organic matter are predicted by the population structure of well-adapted phytoplankton

Shlomit Sharoni and Itay Halevy

Sci Adv **6** (29), eaaw9371.
DOI: 10.1126/sciadv.aaw9371

Science Advances (ISSN 2375-2548) is published by the American Association for the Advancement of Science, 1200 New York Avenue NW, Washington, DC 20005. The title *Science Advances* is a registered trademark of AAAS.